PROCEEDINGS OF SPIE

SPIEDigitalLibrary.org/conference-proceedings-of-spie

Graphene-based 2D-heterostructures for terahertz lasers and amplifiers

D. Yadav, S. Boubanga-Tombet, A. Satou, T. Tamamushi, T. Watanabe, et al.

D. Yadav, S. Boubanga-Tombet, A. Satou, T. Tamamushi, T. Watanabe, T. Suemitsu, H. Fukidome, M. Suemitsu, A. A. Dubinov, V. V. Popov, M. Ryzhii, V. Mitin, M. S. Shur, V. Ryzhii, T. Otsuji, "Graphene-based 2D-heterostructures for terahertz lasers and amplifiers," Proc. SPIE 10917, Terahertz, RF, Millimeter, and Submillimeter-Wave Technology and Applications XII, 109170G (1 March 2019); doi: 10.1117/12.2516494

SPIE.

Event: SPIE OPTO, 2019, San Francisco, California, United States

Graphene-based 2D-heterostructures for terahertz lasers and amplifiers

D. Yadav[a], S. Boubanga-Tombet[a], A. Satou[a], T. Tamamushi[a], T. Watanabe[a], T. Suemitsu[a], H. Fukidome[a], M. Suemitsu[a], A.A. Dubinov[b], V.V. Popov[c], M. Ryzhii[d], V. Mitin[e], M.S. Shur[f], V. Ryzhii[a], and T. Otsuji*[a]

[a] Research Inst. of Electrical Communication, Tohoku University, Sendai, Japan, 9808577
[b] Inst. for Physics of Microstructures, RAS, Nizhny Novgorod, Russia
[c] Kotelnikov Inst. of Radio Engineering and Electronics (Saratov Branch), RAS, Saratov, Russia
[d] Dept. of CSE, University of Aizu, Aizu-Wakamatsu, Japan
[e] Dept. of EE, University at Buffalo, Buffalo, NY, USA
[f] Dept. of ECSE, Rensselaer Polytechnic Institute, Troy, NY, USA

ABSTRACT

This paper reviews recent advances in the terahertz (THz) graphene-based 2D-heterostructure lasers and amplifiers. The linear gapless graphene energy spectrum enables population inversion under optical and electrical pumping giving rise to the negative dynamic conductivity in a wide THz frequency range. We first theoretically discovered these phenomena and recently reported on the experimental observation of the amplified spontaneous THz emission and single-mode THz lasing at 100K in the current-injection pumped graphene-channel field-effect transistors (GFETs) with a distributed-feedback dual-gate structure. We also observed the light amplification of stimulated emission of THz radiation driven by graphene-plasmon instability in the asymmetric dual-grating gate (ADGG) GFETs by using a THz time-domain spectroscopy technique. Integrating the graphene surface plasmon polariton (SPP) oscillator into a current-injection graphene THz laser transistor is the most promising approach towards room-temperature intense THz lasing.

Keywords: Graphene, 2D materials, heterostructures, terahertz, laser, amplifier

1. INTRODUCTION

Studies of carrier interaction in graphene with intense electromagnetic fields [1]-[3]point out to a potential break-through in the speed and frequency performance compared to conventional transistors, photodetectors, modulators, and radiation sources. [4]-[11]. Massless Dirac fermions of electrons and holes in gapless linear symmetric band structures in graphene support the carrier population inversion [12]-[15] and the resultant negative dynamic conductivity in a wide THz frequency range under optical or electrical pumping [12]-[21]. The experimental observations of the THz frequency amplification [22],[23] support the concept of graphene-based THz amplifiers and THz lasers. The room-temperature operating semiconductor THz laser diodes are yet to be developed [10],[24] and their full-scale realization faces a number of challenges. This is why the creation of graphene-based THz amplifiers and THz lasers has been one of the hottest research topics [9], [12]-[21].

Several problems must be addressed to achieve the THz lasing in graphene. The First, interband amplification coefficient of the single pumped graphene layer cannot exceed 2.3% [16], which is directly linked with the universal optical conductivity of graphene [25],[26]. Second, the radiation amplification associated with the direct interband electron transitions competes with the intraband Drude absorption [16], which scales as $1/\omega^2$ at low frequencies ω [27]. Third, carrier-carrier interactions with many body effects dramatically reshape the earliest stage of the ultrafast carrier relaxation in the tens of femtosecond time scale after pumping [28],[29]. This allows for the Auger scattering processes and lowers the carrier population inversion from that for the ideal Dirac fermions [30]-[38]. We recently demonstrated experimental observation of amplified spontaneous THz emission and single-mode THz lasing at 100K in the current-injection pumped graphene-channel field-effect transistors (GFETs) with a distributed-feedback dual-gate structure [39].

*otsuji@riec.tohoku.ac.jp; phone 81 22 217 6104; fax 81 22 217 6104; www.otsuji.riec.tohoku.ac.jp

Terahertz, RF, Millimeter, and Submillimeter-Wave Technology and Applications XII,
edited by Laurence P. Sadwick, Tianxin Yang, Proc. of SPIE Vol. 10917, 109170G
 · doi: 10.1117/12.2516494

The issues of a poor gain overlapping and a low quantum efficiency (limited by the interband absorption coefficient of 2.3%) could be resolved by using the graphene surface plasmon polaritons (SPPs) that could dramatically enhance the interaction between THz photons and graphene due to their nonlinear slow-wave nature [6]-[8], [40]-[47] resulting in a giant enhancement of the THz gain and super-radiant plasmonic lasing in the population-inverted graphene meta-surface structures [48]-[52]. Moreover, the graphene plasmon instability could further enhance the amplification of THz radiation [53]-[56]. This paper is organized as follows. We first review the current-injection graphene THz transistor lasers followed by the discussion of the active graphene SPPs and conclude that integrating the graphene SPP oscillator into a current-injection graphene THz laser transistor is the most promising approach towards room-temperature intense THz lasing.

2. CURRENT-INJECTION GRAPHENE THZ TRANSISTOR LASERS

2.1 Theory and device structure

When the intrinsic graphene is optically pumped with the photon energy $\hbar\Omega$, interband transitions lead to the generation of 'hot' photoelectron-photohole pairs at energy levels $\hbar\Omega/2$ above and below the Dirac point for the electrons and holes, respectively [16]. At room temperature, these photo-excited 'hot' electrons and 'hot' holes are quasi-equilibrated with the low-energy conduction electrons and valence holes around the Dirac point at the ultrafast time scale of tens of femtoseconds due to the carrier-carrier scattering resulting in the quasi-Fermi distribution shown in Fig. 1[9]. As a result, the quasi-Fermi level of electrons and holes split and shift *below* and *above* the Dirac point, respectively. At the same time, the high-energy electrons and holes, lose their energy emit optical phonons. Thus the quasi-Fermi distribution, which is originally widely spread in the energy space, gets concentrated around the Dirac point This results in a rapid recovery of the quasi-Fermi level on a picosecond time scale as shown in Fig. 1 [12],[13]. After the energy relaxation via the optical phonon emissions, the non-equilibrium electrons and holes may lose their energies via the 'interband' optical phonon scattering, impurity-/disordered scattering, as well as the acoustic phonon scattering, or they recombine. Compared to the aforementioned 'intraband' optical phonon scattering, these scattering and recombination processes have much longer relaxation times. Therefore, the nonequilibrium carriers are piled up around the Dirac point if the pumping intensity is sufficiently high, as shown in Fig. 1. This is the carrier population inversion, in which the quasi-Fermi levels for electrons and holes shift *above* and *below* the Dirac point, respectively. The Auger-type three-particle scattering processes are theoretically forbidden in the ideal graphene [28], but they might dominate in the disordered low-quality graphene and/or under an intense pumping leading to significant many-body effects [30]-[38]. Thus, the Auger-type scattering is recognized as a killer of the carrier population inversion [57]. However, the carrier population inversion in the THz frequency range has been experimentally observed even at room temperature in high quality epitaxial graphene after a rather intense optical pumping with a high photon-energy (~1.5 eV) picosecond laser pulses [58]. This result encouraged us to explore the creation of the graphene THz lasers/amplifiers.

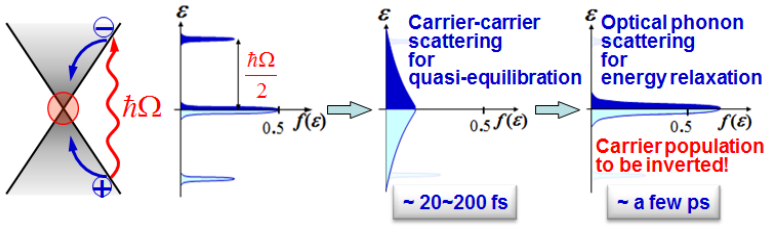

Fig. 1. Nonequilibrium carrier relaxation dynamics in optically pumped intrinsic graphene. (after Ref. [9].)

Optical pumping suffers from a significant heating of the electron-hole plasma suppressing carrier population inversion [20]. However, in the case of the optical pumping with sufficiently low photon energies, the electron-hole plasma can be cooled down [21]. Recently a rigorous theoretical modeling and calculation of the Auger scattering rate including many-body effects of Coulomb interactions reveals that the Auger scattering is substantially suppressed when carrier temperature is maintained at or below room temperature [59]. The current injection pumping is the best way to suppress the carrier heating decreasing the pumping threshold because the pumping energy could be of the order of millielectron volts for p-i-n junctions [17]. Figure 2 shows a dual gate p-i-n structure using a graphene-channel field effect transistor (DG-GFET). The gate biasing ($\pm V_g$) controls the injection level, whereas the drain bias (V_{ds}) controls the level of population inversion. To minimize the undesired tunneling current lowering the injection efficiency the distance between

the dual gate electrodes should be sufficiently long. The conductivity profiles calculated for the typical dimensions and applied bias conditions demonstrate the advantage of current injection compared to the optical pumping [39].

According to Ref. [4], the optical conductivity of graphene channel under the gates and drain biases is given by:

$$\sigma_\omega = \sigma_\omega^{intra} + \sigma_\omega^{inter}, \tag{1}$$

$$\sigma_\omega^{intra} \approx \frac{e^2 \varepsilon_F}{2\pi\hbar^2} \cdot \frac{\tau}{1+\omega^2\tau^2}, \tag{2}$$

$$\sigma_\omega^{inter} \approx \frac{e^2}{2\hbar} \cdot exp\left(\frac{eV - 2e\sqrt{V_F V_g}}{2k_B T}\right) \cdot \sinh\left(\frac{\hbar\omega - eV_{ds}}{2k_B T}\right), \tag{3}$$

where σ_ω^{intra} and σ_ω^{inter} are the intraband and interband component of the conductivity, respectively, e is the elementary charge, ε_F is the Fermi energy reflecting the carrier doping level by applying V_g, $\hbar$ is the reduced Planck constant, τ is the carrier momentum relaxation time, k_B is the Boltzmann constant, and T is the temperature.

Figure 3 shows the simulated σ_ω for typical device geometrical parameters (the gate dielectric thickness of 50 nm, the gate dielectric constant of 4.7) at different V_g, V_{ds}, and τ values. As mentioned above, V_g determines the carrier injection level and the corresponding ε_F, whereas V_{ds} determines the level of the population inversion (the amount of shifting the quasi-Fermi levels of electrons and holes). When the carrier momentum relaxation time is rather long ($\tau = 2.0$ ps) and carrier injection level is relatively low at $V_g = 1.0$V, a weak V_{ds} produces a net gain (negative conductivity) in a wide THz frequency range. When the carrier injection level increases to $V_g = 5.0$V, the upper cutoff frequency to obtain a net gain increases although a larger V_{ds} is needed to produce a net gain. The lower cutoff frequency of the net gain exhibits the blue-shifting. For both cases when the V_{ds} increases far above ε_F, the potential slope along the channel results in the reduction of the carrier injection and corresponding gain (not shown in Fig. 3) [21]. Thus, the lower and upper threshold levels to get the net gain coexist. The situation dramatically changes when the value of τ becomes short (down to 0.1 ps); in this case, the net gain almost disappears. This result clearly indicates that the high-quality graphene having the value of τ on the order of a picosecond is needed to obtain a net gain in the THz range.

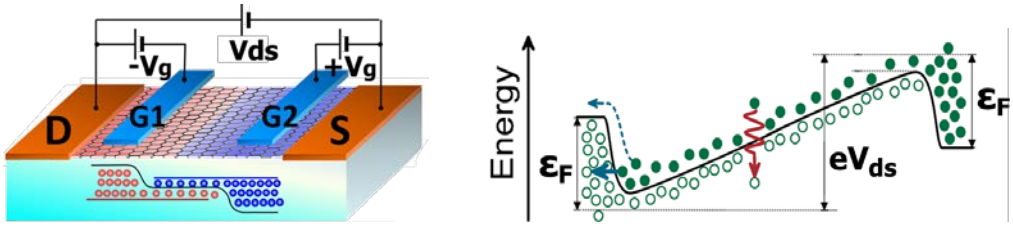

(a) (b)

Fig. 2. Schematic cross-sectional view (a) and corresponding energy band diagram (b) of a lateral p-i-n junction in a DG-GFET for current-injection lasing.

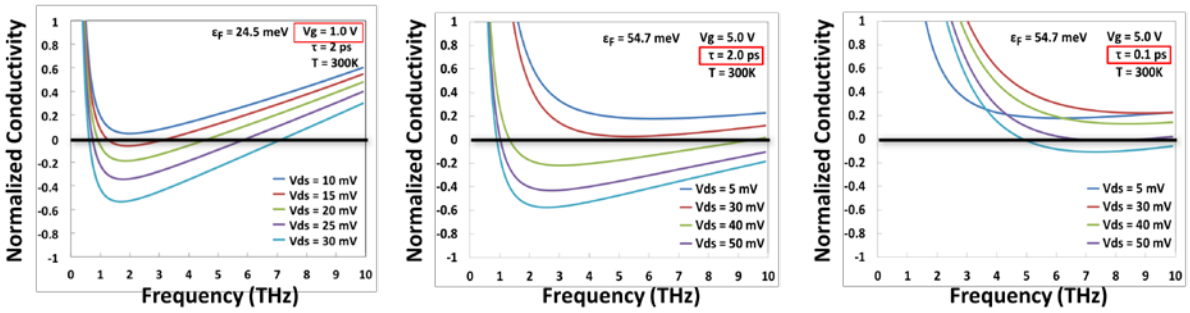

Fig. 3. Simulated optical conductivity for a DG-GFET structure at different V_g, V_{ds} and τ values. The gate dielectric thickness and constant are assumed to be 50 nm and 4.7, respectively. (after Ref. [39].)

2.2 Experimental results and discussion

The graphene used for our experiments was synthesized by the thermal decomposition of a C-face 4H-SiC substrate [60]. The Raman spectrum confirmed a high-quality, a few layer non-Bernal stacked graphene [39]. The GFET was fabricated using a standard photolithography and a gate stack with a SiN dielectric layer (see Fig. 4(a)) providing an excellent intrinsic field-effect mobility exceeding 100,000 cm^2/Vs at 300K at the maximal transconductance [39]. A pair of teeth-brash-shaped gate electrode was patterned to form a distributed feed-back (DFB) cavity in which the active gain area and corresponding gain coefficient were spatially modulated as shown in Fig. 4(b).The grating period Λ, the effective refractive index n_{eff}, the Bragg wavelength λ_B, and the principal mode f_P were 12 μm, 2.52, 60.5 μm, and 4.96 THz, respectively. The fabricated DFB-DG-GFETs exhibited an ambipolar behavior in the current-to-gate voltages (V_{g1}, V_{g2}) characteristics (see Fig. 4(c)). The slope of the ambipolar curve got steeper at lower temperatures, reflecting the longer τ values at lower temperatures [39].

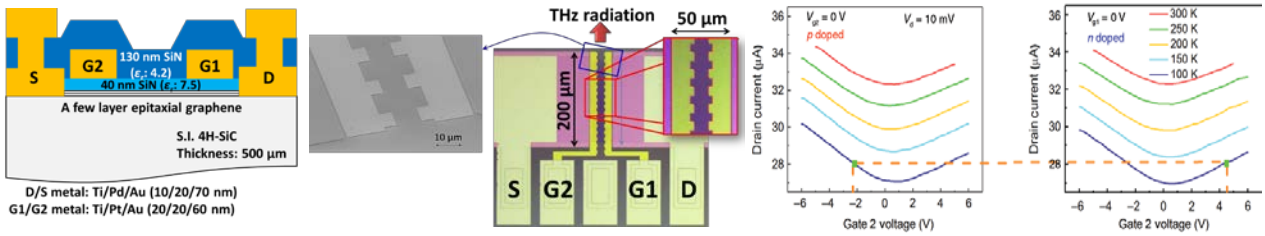

(a) (b) (c)

Fig. 4. Fabricated DFB-DG-GFET [39]. (a) Device cross-section. (b) Device SEM and photo images. (c) Measured ambipolar current-voltage characteristics for a fabricated DFB-DG-GFET. (after Ref. [39].)

The THz emission was measured at temperatures from 300K down to 100K using a Fourier-transform spectrometer with a 4.2K-cooled Si bolometer. The background blackbody radiation was observed under the zero-bias condition and was subtracted from the radiation observed under biased conditions. One sample exhibited rather strong emission at 100K (Fig. 5(a)), stronger than that at higher temperatures from 150 to 300K (Fig. 5(b)) The emission was observed in 1-7.6 THz range when V_d was forward-biased to a certain level under symmetric electron and hole injection conditions (V_{g2} = 4.56 V, V_{g1} = -2.58 V) leading to the carrier population inversion. The first peak at ~2 THz came from the original gain spectral profile as shown in Fig. 3(b), whereas the second peak at ~5 THz coincided with the fundamental DFB mode. The substrate-thickness dependent THz photon field distribution could not meet the maximal available gain-overlapping condition. As a result, the single-mode lasing was transcended from the spontaneous broadband THz emission to the single-mode stimulated emission. Apart from temperature dependent spontaneous THz emission, the device also exhibited double-threshold-like behavior with the maximal emission intensity ~80 μW as shown in Fig. 5(c), which may be due to the carrier overcooling effect [19],[20].

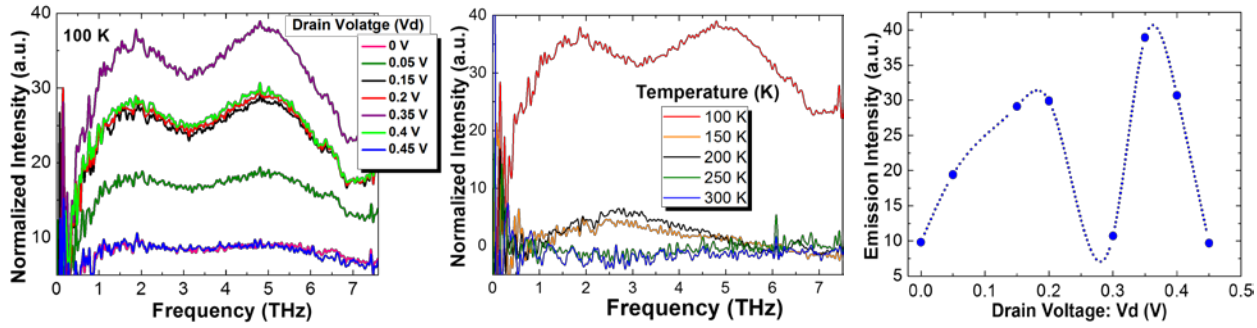

(a) (b) (c)

Fig. 5. (a) Observed emission spectra in a different DFB-DG-GFET sample under population inversion (V_{g2}=4.56 V, V_{g1}= -2.58 V) for different values of drain voltage at 100K. (b) Temperature dependence of the emission spectra. (c) THz emission intensity vs. drain voltage (V_d) at 100K. (after Ref. [39].)

The experiment was conducted for different samples having similar design geometries and fabricated on the identical wafer. The observed emission spectra at 100K are plotted in Figs. 6(a) and (b). The emission spectra contain huge

systematic noise at around 3.6-4.2 THz due to the misalignment of the Martin-Puplett interferometer (disregarded as shown in Fig. 6(a)). No distinctive emission was observed at 300 K, but a rather sharp single mode emission at 5.2 THz was observed at 100K when V_{ds} is positively applied to a certain level under symmetric electron and hole injection conditions (see Figs. 6a and 6b). As was observed in case of aforementioned amplified broadband spontaneous emission, the single mode emission also exhibited a non-monotonic threshold-like behavior (see Fig. 6(c)) with the highest intensity ~0.1 μW. Spectral narrowing with increasing the carrier injection around the threshold was also observed. The emission spectra at V_{ds} = 0.5 V could fit to the Lorentzian curve with the Q factor of 170 (a linewidth of 30.6 GHz), which agrees well with the simulated results [39].

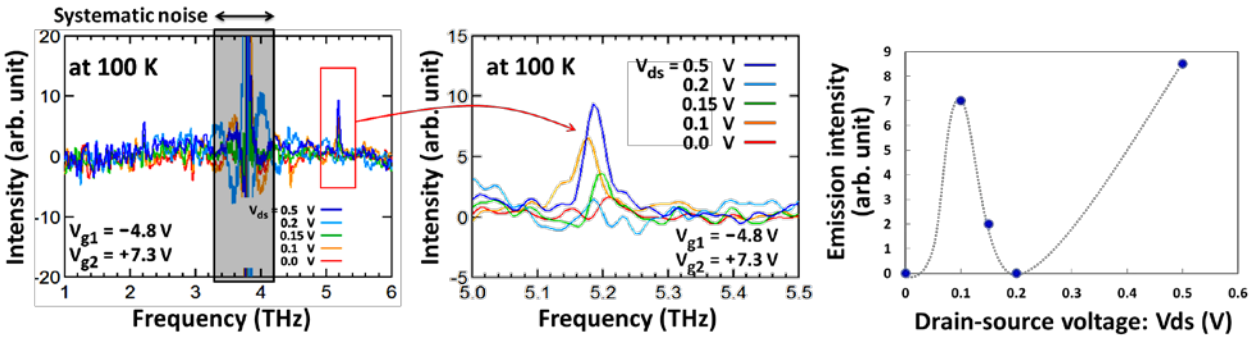

Fig. 6. Observed emission spectra at 100K (a) in a broad range and (b) in a magnified range at around 5.2 THz. (after Ref. [39].)

The conductivity analysis using Eqs. (1) to (3) suggests that much higher Q factors, (i.e. a higher graphene material having longer momentum relaxation times) are needed to enable the single-mode intense lasing at room temperature. The Q factors of the DFB structure can be further increased by orders of magnitude by increasing the number of the DFB periods as well as by introducing a thick dielectric layer on top of the device to maximize the spontaneously-emitted THz photon field at the graphene channel area [39]. These improvements will be the subjects of future studies.

3. GRAPHENE ACTIVE SURFACE PLASMON POLARITONS

3.1 Giant gain enhancement via graphene plasmon polaritons

The collective charge density waves (which are called 'plasma waves') in graphene are excited by an electromagnetic irradiation. The excitations of the graphene plasmons can help resolve the issues of the poor gain overlapping and low quantum efficiency (limited by the interband absorption coefficient of 2.3%) in the current-injection DFB-DGGFETs. The graphene 2D plasmons have been intensively studied theoretically and experimentally [7]-[11],[40]-[45]. The group velocity of graphene 2D plasmons is on the order of 10^6 m/s, which is two orders of magnitude lower than the speed of light. Due to such a 'slow-wave' nature, the graphene 2D plasmons mediate the light-matter interactions. The THz electromagnetic radiation impinging onto the graphene surface excites the 2D surface plasmons. The TM (transverse magnetic) mode THz photons are coupled with 2D plasmons forming SPPs) propagating along the in-plane component of the incident THz photon radiation vectors as shown in Fig. 7(a). In such a situation, the propagation of the SPPs will lead to one of the two distinctive scenarios corresponding to a 'giant loss' or a 'giant gain', depending on the 'polarity' of the conductivity. When graphene is semi-metallic or semi-conductive with a specific 'positive' conductivity value, the SPP propagation can drastically enhance the interaction between the THz photons and graphene, resulting in an extremely strong 'absorption' of the incident THz photon energy [8]. This is the case of the 'giant loss.'

On the contrary, when graphene-carrier populations are inverted via optical pumping and the resultant gain is negative in the THz range, the SPP propagation results in an extremely strong 'amplification' of the incident THz photon energy. This is the case of the 'giant gain.' The authors' group first theoretically discovered this phenomenon [49] (see Figs. 7(b) and (c) and then observed it experimentally [52]. The simulated results demonstrate the orders of magnitude enhancement of the gain coefficient ranging up to the order of 10^4 cm^{-1} in a wide THz range, more than four orders of magnitude larger than the cases when the SPPs are not excited [49]. As is described in detail in Ref. [52], the optical-pump, THz-probe and optical-probe measurement was conducted at room temperature for intrinsic monolayer graphene exfoliated from graphite and transferred onto a SiO_2/Si substrate. The experiment was based on the time-resolved near-field reflective electrooptic sampling with fs-IR laser pulse for optical pumping and a synchronously generated THz

pulse for probing the THz dynamics of the sample in a THz photon-echo manner. The observed gain enhancement factor within the measurable limited frequency range up to 4 THz was ~50, in fair agreement with the theoretical calculations shown in Fig. 7 [52].

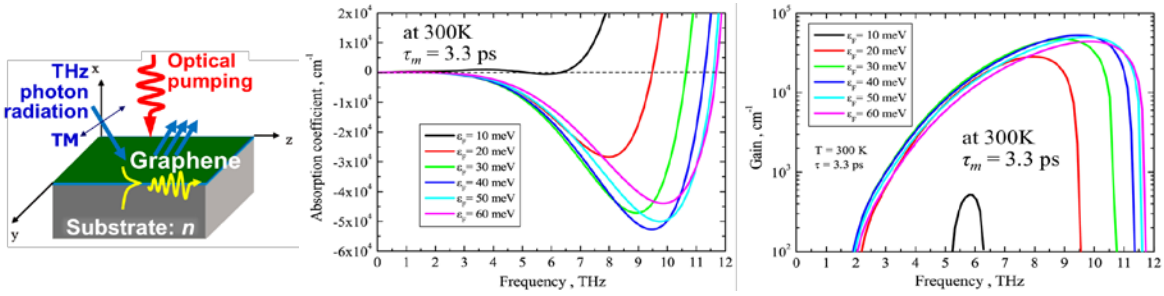

(a) (b) (c)

Fig. 7. Excitation of the SPPs in optically pumped graphene. (a) Schematic view. Simulated frequency dependences of SPP absorption (b) and gain (c) for monolayer population-inverted graphene on SiO_2/Si substrate at 300K for different levels of population inversion (given by the quasi-Fermi energy ε_F = 10, 20, 30, 40, 50, 60 meV). (after Ref. [52].)

3.2 Superradiant plasmonic lasing in population-inverted graphene

The amplification of THz waves by stimulated generation of resonant SPPs in a planar periodic array of graphene plasmonic microcavities will be another scenario theoretically proposed in Refs. [50] and [51]. When a grating-type gate stack is incorporated into planar graphene such as in an asymmetric dual-grating-gate graphene-channel field-effect transistor (ADGG-GFET) structure (see Fig. 8(a)) the gain is resonantly and cooperatively enhanced [51]. The graphene could be pumped either by optical pumping or by the injection of the electrons and holes from the ADGG electrodes. In the latter case, (see Fig. 2) the two pairs of the adjacent ADGG fingers work as the carrier-injection element, and the graphene area beneath the wider space (width d_2) exhibits the carrier-population inversion under the complementary ADGG-biased and weakly drain-source forward biased conditions (see Fig. 8(b)). Therefore, one can expect spontaneous THz photon emission (see Fig. 5). The important feature of the ADGG-GFET structure is the periodically arrayed gain sections in which the unit gain area defines the SPP resonant modes according to its microcavity size d_2 and carrier densities. If the ADGG-GFET is installed in a Fabry-Perot-like vertical photonic cavity, the spontaneously emitted THz photons will be fed back to graphene, stimulating the resonantly SPP-induced THz emission. Since the ADGG works as a broadband antenna that can convert non-radiative SPPs to the radiative photons one can expect a resonantly enhanced coherent THz photon emission. If the Fabry-Perot longitudinal modes match the 2D plasmon modes, the cooperative stimulated plasmon/photon emission of THz radiation should result in an intense THz lasing. Recent studies revealed the occurrence of superradiant SPP THz lasing in such an ADGG GFET structure with feature size of the order of micrometers [51]. The carrier population and hence the graphene optical conductivity are characterized by the quasi Fermi levels and carrier temperature [50],[51]. Fig. 8(c) shows typical simulated gain values versus frequency.

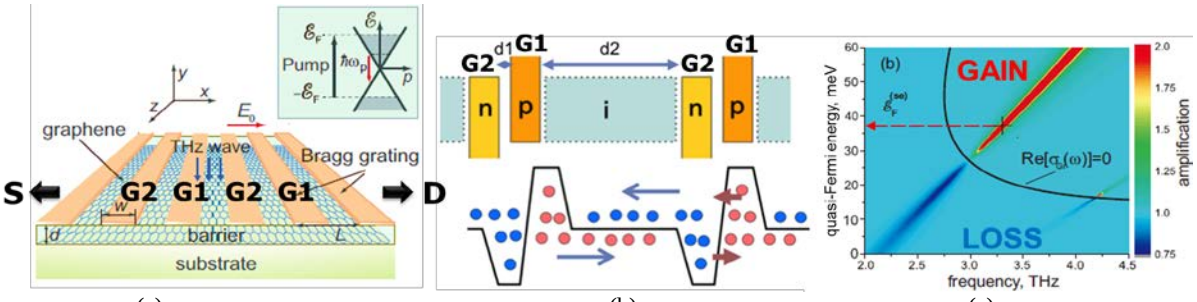

(a) (b) (c)

Fig. 8. ADGG-GFET as a graphene plasmonic lasing device. (a) Device structure. (b) Carrier injection in a unit gain section under complementary ADGG biased and weakly drain-source forward biased conditions. (c) Simulated. (after Ref. [51].)

The SPPs in different graphene microcavities oscillate in phase (even without the incoming electromagnetic wave) because the metal contacts act as the synchronizing elements between the adjacent graphene microcavities. (A mechanical analogy is the chain of rigid crossbars connecting oscillating springs). Therefore, the plasma oscillations in the array of graphene microcavities constitute a single collective plasmon mode distributed over the entire area of the

array. This leads to the enhanced *superradiant* electromagnetic emission from the array. Such extraordinary properties of a collective mode in an array of synchronized oscillators are well known in optics: the power of electromagnetic emission from such an array grows as the square of the number of the oscillators in the array [50].

3.3 Graphene-plasmon instabilities for light amplification of stimulated emission of THz radiation

The generation and amplification of electromagnetic waves by the current-driven plasmon instabilities in graphene are other possible mechanisms to obtain the giant THz gain enhancement effect [53]-[56]. We have investigated dc current driven plasmonic instabilities in ADGG-GFETs high mobility graphene metamaterials (see Figs. 9(a) and (b)) [54]. When gate 1 (G1) is biased higher to attract electrons and gate 2 (G2) is biased at the Dirac voltage to deplete electrons, the graphene channel region underneath G1 works as an SPP cavity whereas the graphene channel region underneath G2 works as a high-impedance section. Such a G1/G2 biased ADGG-GFET resonantly absorbs the incident THz radiation when drain is unbiased.

Under such G1/G2 bias condition, the application of the drain-to-source dc bias voltage leads to a constant drain-to-source dc channel current flow. Due to an asymmetric DGG layout (the left-side space *S*g1 and the right-side space *S*g2 from G1 to G2 finger are different; *S*g1 < *S*g2 in Fig. 9(a)), the impedance at the right-side boundary of the plasmonic cavity is higher than that at the left-side boundary of the plasmonic cavity. Such an asymmetrical boundary condition may promote the Doppler-shift-type Dyakonov-Shur (DS) plasmonic instability [61]. At the same time to make the current continuity throughout the channel region, the electron drift velocity is spatially and periodically modulated: a higher velocity underneath G2 and a lower velocity underneath G1. Thus high-velocity electrons are injected to the low-velocity plasmonic cavity region which may excite the plasmons in a resonant manner. This also leads to the electron-transit-time-modulation-type Ryzhii-Satou-Shur (RSS) plasmonic instability [62],[63]. The former DS instability has a broadband nature whereas the latter RSS instability may have a resonant nature when the plasmon mode frequencies coincide with the electron bunching frequencies. We numerically simulated the time evolution of the electric field intensities around the channel region and observed the occurrence of self-oscillatory instabilities shown in Figs. 9(c) and (d) [54].

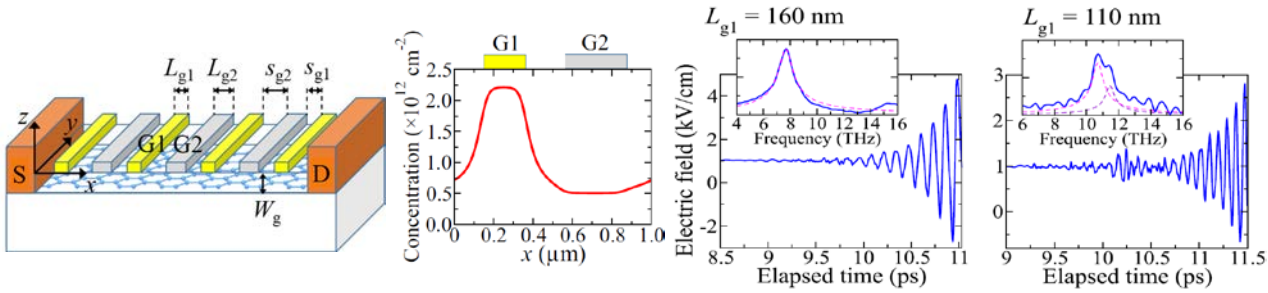

Fig. 9. (a) Schematic views of a ADGG-GFET. (b) A profile of steady-state electron concentration in a unit section of the ADGG-GFET channel under consideration. Time evolution of the electric field at the middle of a channel region under G2 with (c) L_{g1} = 160 nm and (d) L_{g1} = 110 nm. The external electric field is set to E_{ext} = 0.8 kV/cm. The insets show the corresponding absolute values of the Fourier transform. (after Ref. [54].)

We have recently succeeded in experimental observation of light amplification of stimulated emission of THz radiation driven by graphene-plasmon instability in ADGG-GFETs by using a THz time-domain spectroscopy technique [64]. With increasing the drain dc bias level, the absorption peak exhibited a red shift and weakened. When the drain bias approached a low-end threshold level, the sample became perfectly transparent over the measured frequency range. The most striking observed phenomenon was a resonant amplification with the maximum gain of 9% when the drain bias exceeded a high-end threshold level, exhibiting a blue shift with increasing the drain bias. Such an overall response from absorption to amplification with respect to the drain bias agrees well with the graphene plasmon instability theory [64].

4. CONCLUSION

Linear and gapless energy spectrum of graphene carriers enables population inversion under optical and electrical pumping giving rise to negative dynamic conductivity in a wide THz frequency range. We first theoretically discovered this phenomena and resultant THz gain and recently observed the amplified spontaneous THz emission and single-mode THz lasing at 100K in the current-injection pumped GFETs with the DFB-DG structure. The present issues of poor gain

overlapping and low quantum efficiency (limited by the interband absorption coefficient of 2.3%) could be resolved by using the graphene SPPs that could dramatically enhance the THz gain due to their nonlinear slow-wave nature. The graphene-SPP instability driven light amplification of the stimulated emission of the THz radiation is feasible. Integrating the graphene SPP oscillator/amplifier into a current-injection graphene THz laser transistor will be a possible smart solution towards achieving the room-temperature intense THz lasing.

ACKNOWLEDGEMENTS

The authors thank J. Mitsushio, K. Sugawara, Y. Yabe, T. Fukushima, Y. Tobah, D. Svintsov, O. Polischuk, V. Ya Aleshkin, K. Maussang, D. But, and W. Knap for their contributions. The authors also thank S. Mikhailov for his valuable discussion. This work was supported by JSPS KAKENHI #16H06361, #16K14243, and 18H05331, Japan. The work at RPI was supported by the US Army Research Laboratory and by the US Office of Naval Research.

REFERENCES

[1] Novoselov, K.S., Geim, A.K., Morozov, S.V., Jiang, D., Zhang, Y., Dubonos, S.V., Grigorieva, I.V., Frisov, A.A., "Electric field effect in atomically thin carbon films," *Science* **306**, 666-669 (2004).
[2] Novoselov, K.S., Geim, A.K., Morozov, S.V., Jiang, D., Katsnelson, M.I., Grigorieva, I.V., Dubonos, S.V., Firsov, A.A., "Two-dimensional gas of massless Dirac fermions in graphene," *Nature* **438**, 197-200 (2005).
[3] Zhang, Y., Tan, Y.-W., Stormer, H.L., Kim, P., "Experimental observation of the quantum Hall effect and Berry's phase in graphene," *Nature* **438**, 201-204 (2005).
[4] Geim, A.K., Novoselov, K.S., "The rise of graphene," *Nat. Mater.* **26**, 183-191 (2007).
[5] Schwierz, F., "Graphene transistors," *Nature Nanotech.* **5**, 487–496 (2010).
[6] Bonaccorso, B., Sun, Z., Hasan, T., and Ferrari, A.C., "Graphene photonics and optoelectronics," *Nature Photon.* **4**, 611-622 (2010).
[7] Bao, Q., and Loh, K.P., "Graphene photonics, plasmonics, and broadband optoelectronic devices," *ACS Nano* **6**, 3677–3694 (2012).
[8] Grigorenko, A.N., Polini, M., and Novoselov, K.S., "Graphene plasmonics," *Nature Photon.* **6**, 749-759 (2012).
[9] Otsuji, T., Boubanga-Tombet, S.A., Satou, A., Fukidome, H., Suemitsu, M., Sano, E., Popov, V., Ryzhii, M., and Ryzhii, V., "Graphene-based devices in terahertz science and technology," *J. Phys. D: Appl. Phys.* **45**, 303001 (2012).
[10] Tredicucci, A., and Vitiello, M.S., "Device concepts for graphene-based terahertz photonics," *IEEE J. Sel. Top. Quantum Electron.* **20**, 8500109 (2014).
[11] Hartmann, R.R., Kono, J., and Portnoi, M.E., "Terahertz science and technology of carbon nanomaterials," *Nanotechnol.* **25**, 322001 (2014).
[12] Satou, A., Vasko, F.T., and Ryzhii, V., "Nonequilibrium carriers in intrinsic graphene under interband photoexcitation," *Phys. Rev. B* **78**, 115431 (2008).
[13] Sano, E., "Monte Carlo simulation of ultrafast electron relaxation in graphene," *Appl. Phys. Exp.* **4**, 085101 (2011).
[14] Gierz, I., Petersen. A., Mitrano, M., Cacho, C., Springate, E., Stuhr, A., Kuhler, A., and Starke, U., "Snapshots of non-equilibrium Dirac carrier distributions in graphene," *Nat. Mater.* **12**, 1119-1124 (2013).
[15] Winzer, T., Malic, E., and Knorr, A., "Microscopic mechanism for transient population inversion and optical gain in graphene," *Phys. Rev. B* **87**, 165413 (2013).
[16] Ryzhii, V., Ryzhii, M., and Otsuji, T., "Negative dynamic conductivity of graphene with optical pumping," *J. Appl. Phys.* **101**, 083114 (2007).
[17] Ryzhii, M., and Ryzhii, V., "Injection and population inversion in electrically induced p-n junction in graphene with split gates," *Jpn. J. Appl. Phys.* **46**, L151-L153 (2007).
[18] Ryzhii, V., Dubinov, A., Otsuji, T., Mitin, V., and Shur, M.S., "Terahertz lasers based on optically pumped multiple graphene structures with slot-line and dielectric waveguides," *J. Appl. Phys.* **107**, 054505 (2010).
[19] Ryzhii, V., Ryzhii, M., Mitin, V., Satou, A., and Otsuji, T., "Effect of heating and cooling of photogenerated electron–hole plasma in optically pumped graphene on population inversion," *Jpn. J. Appl. Phys.* **50**, 094001 (2011).

[20] Ryzhii, V., Ryzhii, M., Mitin, V., Otsuji, T., "Toward the creation of terahertz graphene injection laser," *J. Appl. Phys.* **110**, 094503 (2011).
[21] Ryzhii, V., Semenikhin, I., Ryzhii, M., Svintsov, D., Vyurkov, V., Satou, A., and Otsuji, T., "Double injection in graphene p-i-n structures," *J. Appl. Phys.* **113**, 244505 (2013).
[22] Boubanga-Tombet, S., Chan, S., Watanabe, T., Satou, A., Ryzhii, V., and Otsuji, T., *Phys. Rev. B* **85**, 035443 (2012).
[23] Li, T., Luo, L., Hupalo, M., Zhang, J., Tringides, M.C., Schmalian, J., and Wang, J., "Femtosecond population inversion and stimulated emission of dense Dirac Fermions in graphene," *Phys. Rev. Lett.* **108**, 167401 (2012).
[24] Tonouchi, M., "Cutting-edge terahertz technology," *Nature Photon.* **1**, 97–105 (2007).
[25] Falkovsky, L.A., Varlamov, A.A., "Space-time dispersion of graphene conductivity," *Eur. Phys. J. B* **56**, 281-284 (2007).
[26] Mak, K.F., Sfeir, M.Y., Wu, Y., Lui, C.H., Misewich, J.A., and Heinz, T.F., "Measurement of the optical conductivity of graphene," *Phys. Rev. Lett.* **101**, 196405 (2008).
[27] Martl, M., Darmo, J., Deutsch, C., Brandstetter, M., Andrews, A.M., Klang, P., Strasser, G., and Unterrainer, K., "Gain and losses in THz quantum cascade laser with metal-metal waveguide," *Opt. Exp.* **19**, 733-738 (2011).
[28] Foster, M.S., and Aleiner, I.L., "Slow imbalance relaxation and thermoelectric transport in graphene," *Phys. Rev. B* **79**, 085415 (2009).
[29] Kotov, V.N., "Electron-Electron Interactions in Graphene: Current Status and Perspectives," *Rev. Mod. Phys.* **84**, 1067-1125 (2012).
[30] Tomadin, A., Brida, D., Cerullo, G., Ferrari, A.C., and Polini, M., "Nonequilibrium dynamics of photoexcited electrons in graphene: Collinear scattering, Auger processes, and the impact of screening," *Phys. Rev. B* **88**, 035430 (2013).
[31] Brida, D., Tomadin, A., Manzoni, C., Kim, Y.J., Lombardo, A., Milana, S., Nair, R.R., Novoselov, K.S., Ferrari, A.C., Cerullo, G., and Polini, M., "Ultrafast collinear scattering and carrier multiplication in graphene," *Nature Comm.* **4**, 1987 (2013).
[32] Rana, F., "Electron-hole generation and recombination rates for Coulomb scattering in graphene," *Phys. Rev. B* **76**, 155431 (2007).
[33] Strait, J.H., Wang, H., Shivaraman, S., Shields, V., Spencer, M., and Rana, F., "Very slow cooling dynamics of photoexcited carriers in graphene observed by optical-pump terahertz-probe spectroscopy," *Nano Lett.* **11**, 4902-4906 (2011).
[34] Winzer, T., Knorr, A., and Malic, E., "Carrier multiplication in graphene," *Nano Lett.* **10**, 4839-4843 (2010).
[35] Winzer, T., and Malic, E., "Impact of Auger processes on carrier dynamics in graphene," *Phys. Rev. B* **85**, 241404(R) (2012).
[36] Obraztsov, P.A., Rybin, M.G., Tyurnina, A.V., Garnov, S.V., Obraztsova, E.D., Obraztsov, A.N., and Svirko, Y.P., "Broadband light-induced absorbance change in multilayer graphene," *Nano Lett.* **11**, 1540-1545 (2011).
[37] Tani, S., Blanchard, F., and Tanaka, K., "Ultrafast carrier dynamics in graphene under a high electric field," *Phys. Rev. Lett.* **99**, 166603 (2012).
[38] Siegel, D.A., Parka, C.-H., Hwangb, C., Deslippe, J., Fedorov, A.V., Louie, S.G., and Lanzar, A., "Many-body interactions in quasi free-standing graphene," *Proc. Natl. Acad. Sci.* USA **108**, 11365-11369 (2011).
[39] Yadav, D., Tamamushi, G., Watanabe, T., Mitsushio, J., Tobah, Y., Sugawara, K., Dubinov, A.A., Satou, A., Ryzhii, M., Ryzhii, V., and Otsuji, T., "Terahertz light-emitting graphene-channel transistor toward single-mode lasing," *Nanophoton*. **7**, 741-752 (2018).
[40] Ryzhii, V., Satou, A., and Otsuji, T., "Plasma waves in two-dimensional electron-hole system in gated graphene heterostructures," *J. Appl. Phys* **101**, 024509 (2007).
[41] Hwang, E.H., and Das Sarma, S., "Dielectric function, screening, and plasmons in two-dimensional graphene," *Phys. Rev. B* **75**, 205418 (2007).
[42] Das Sarma, S., and Hwang, E.H., "Plasmons in coupled bilayer structures," *Phys. Rev. Lett.* **81**, 4216-4219 (1998).
[43] Hwang, E.H., and Das Sarma, S., "Plasmon modes of spatially separated double-layer graphene," *Phys. Rev. B* **80**, 205405 (2009).
[44] Jablan, M., Buljan, H., and Soljačić, M., "Plasmonics in graphene at infrared frequencies," *Phys. Rev. B* **80**, 245435 (2009).
[45] Koppens, F.H.L., Chang, D.E., and García de Abajo, F.J., "Graphene plasmonics: a platform for strong light–matter interaction," *Nano Lett.* **11**, 3370-3377 (2011).

[46] Rana, F., Strait, J.H., Wang, H., and Manolatou, C., "Ultrafast carrier recombination and generation rates for plasmon emission and absorption in graphene," *Phys. Rev. B* **84**, 045437 (2011).
[47] Svintsov, D., Vyurkov, V., Yurchenko, S., Otsuji, T., and Ryzhii, V., "Hydrodynamic model for electron-hole plasma in graphene," *J. Appl. Phys.***111**, 083715 (2012).
[48] Rana, F., "Graphene terahertz plasmon oscillators," *IEEE Trans. Nanotechnol.* **7**, 91-99 (2008).
[49] Dubinov, A.A., Aleshkin, V.Y., Mitin, V., Otsuji, T., and Ryzhii, V., "Terahertz surface plasmons in optically pumped graphene structures," *J. Phys. Condens. Matter* **23**, 145302 (2011).
[50] Popov, V.V., Polischuk, O.V., Davoyan, A.R., Ryzhii, V., Otsuji, T., and Shur, M.S., "Plasmonic terahertz lasing in an array of graphene nanocavities," *Phys. Rev. B* **86**, 195437 (2012).
[51] Popov, V.V., Polischuk, O.V., Nikitov, S.A., Ryzhii, V., Otsuji, T., and Shur, M.S., "Amplification and lasing of terahertz radiation by plasmons in graphene with a planar distributed Bragg resonator," *J. Opt.* **15**, 114009 (2013).
[52] Watanabe, T., Fukushima, T., Yabe, Y., Boubanga Tombet, S.A., Satou, A., Dubinov, A.A., Aleshkin, V.Y., Mitin, V., Ryzhii, V., and Otsuji, T., "The gain enhancement effect of surface plasmon polaritons on terahertz stimulated emission in optically pumped monolayer graphene," *New J. Phys.* **15**, 075003 (2013).
[53] Tomadin, A., and Polini, M., "Theory of the plasma-wave photoresponse of a gated graphene sheet," *Phys. Rev. B* **88**, 205426-1-10 (2013).
[54] Koseki, Y., Ryzhii, V., Otsuji, T., Popov, V.V., and Satou, A., "Giant plasmon instability in dual-grating-gate graphene field-effect transistor," *Phys. Rev. B* **93**, 245408-1-5 (2016).
[55] Aryal, C.M., and Hu, B.Y.-K., "Plasma wave instabilities in nonequilibrium graphene," *Phys. Rev. B* **94**, 115401-1-9 (2016)
[56] Kaminer, I., Katan, Y.T., Buljan, H., Shen, Y., Ilic, O., López, J.J., Wong, L.J., Jonnopoulos, J.D., and Soljačić, M., "Efficient plasmonic emission by the quantum Čerenkov effect from hot carriers in graphene," *Nat. Comm.* **7**, 11880-1-9 (2016).
[57] Kim, R., Pereveinos, V., and Avouris, P., "Relaxation of optically excited carriers in graphene," *Phys. Rev. B* **84**, 075449-1- (2011).
[58] Someya, T., Fukidome, H., Watanabe, H., Yamamoto, T., Okada, M., Suzuki, H., Ogawa, Y., Iimori, T., Ishii, N., Kanai, T., Tashima, K., Feng, B., Yamamoto, S., Itatani, J., Komori, F., Okazaki, K., Shin, S., and Matsuda, I., "Suppression of supercollision carrier cooling in high mobility graphene on SiC(0001)," *Phys. Rev. B* **95**, 165303-1-7 (2017).
[59] Alymov, G., Vyurkov, V., Ryzhii, V., Satou, A., and Svintsov, D., "Auger recombination in Dirac materials: a tangle of many-body effects," *Phys. Rev. B* **97**, 205411-1-13 (2018).
[60] Fukidome, H., Kawai, Y., Fromm, F., Kotsugi, M., Handa, H., Ide, T., Ohkouchi, T., Miyashita, H., Enta, Y., Kinoshita, T., Seyller, T., and Suemitsu, M., "Precise control of epitaxy of graphene by microfabricating SiC substrate," *Appl. Phys. Lett.* **101**, 041605 (2012).
[61] Dyakonov, M. and Shur, M., "Shallow water analogy for a ballistic field effect transistor: New mechanism of plasma wave generation by dc current," *Phys. Rev. Lett.* **71**, 2465-2468 (1993).
[62] Ryzhii, V., Satou, A., and Shur, M., "Plasma Instability and Terahertz generation in HEMTs due to electron transit-time effect," *IEICE Trans. Electron.* **E89-C**, 1012-1019 (2006).
[63] Ryzhii, V., Satou, A., Ryzhii, M., Otsuji, T., and Shur, M.S., "Mechanism of self-excitation of terahertz plasma oscillations in periodically double-gated electron channels," *J. Phys.: Condens. Matter* **20**, 384207 (2008).
[64] Boubanga-Tombet, S., Yadav, D., Knap, W., Popov, V.V., and Otsuji, T., "Plasmonic instabilities and terahertz waves amplification in graphene metamaterials," *arXiv*:1801.04518 (2018).